Supplementary Information

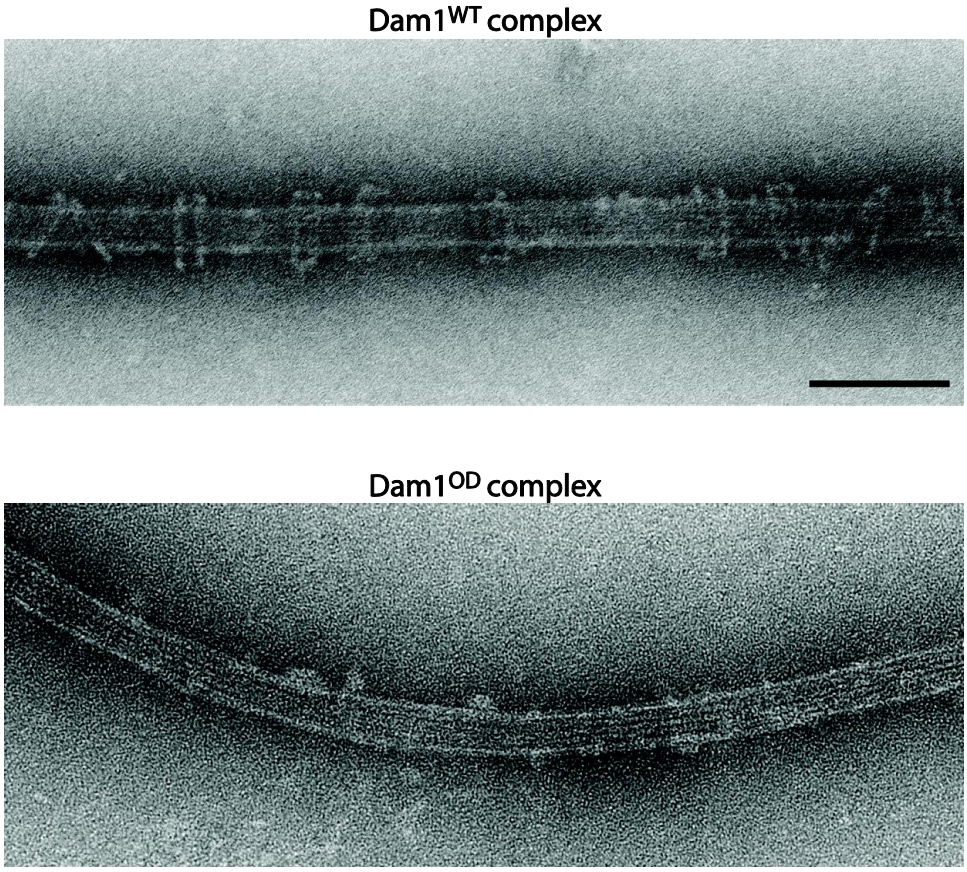

Supplementary Figure 1. The Dam1^{OD} complex does not form oligomeric rings around microtubules.
Negative-stain electron micrographs of Dam1^{WT} complex (top) and Dam1^{OD} complex (bottom) on taxol-stabilized microtubules. Scale bar is 100 nm applies to both panels. Image levels were adjusted for visual clarity.

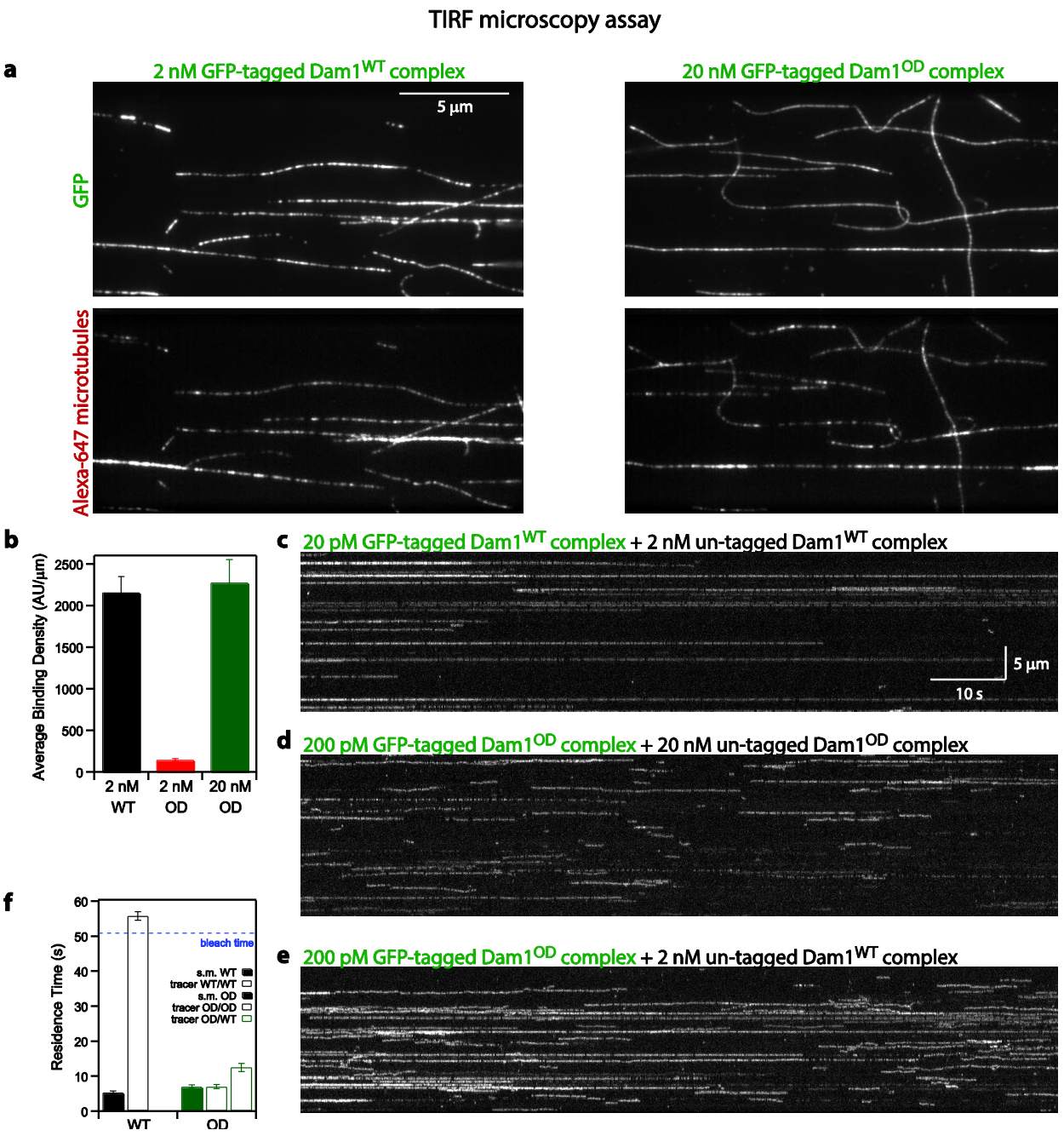

Supplementary Figure 2. The Dam1^{OD} complex lacks the ability to oligomerize on microtubules.

(a) TIRF microscopy images of 2 nM GFP-tagged wild-type (left panels) and 20 nM GFP-tagged oligomerization-deficient (right panels) Dam1 complex on Alexa-647-labeled microtubules. Top: GFP channel; Bottom: Alexa-647 channel. (b) Average binding density of GFP-tagged Dam1 complex on microtubules. To match binding density, Dam1^{OD} complex was added at 10-fold higher concentration than Dam1^{WT} complex. (c-e) Single molecules were imaged in conditions shown in (a) by mixing GFP-tagged and un-tagged Dam1 complexes. (f) Residence times for

“true” single-molecule conditions (solid bars, $Dam1^{WT}$ or $Dam1^{OD}$ complex at 5-40 pM on microtubules, data from Fig. 1c) are compared to the residence times for “tracer” single-molecules (striped bars) in the conditions shown in (c-e). Dashed blue line indicates the average time for single fluorophores to photobleach under identical imaging conditions. Error bars in (b) indicate s.e.m.; in (e), error was estimated using bootstrapping analysis as in Fig. 1c.

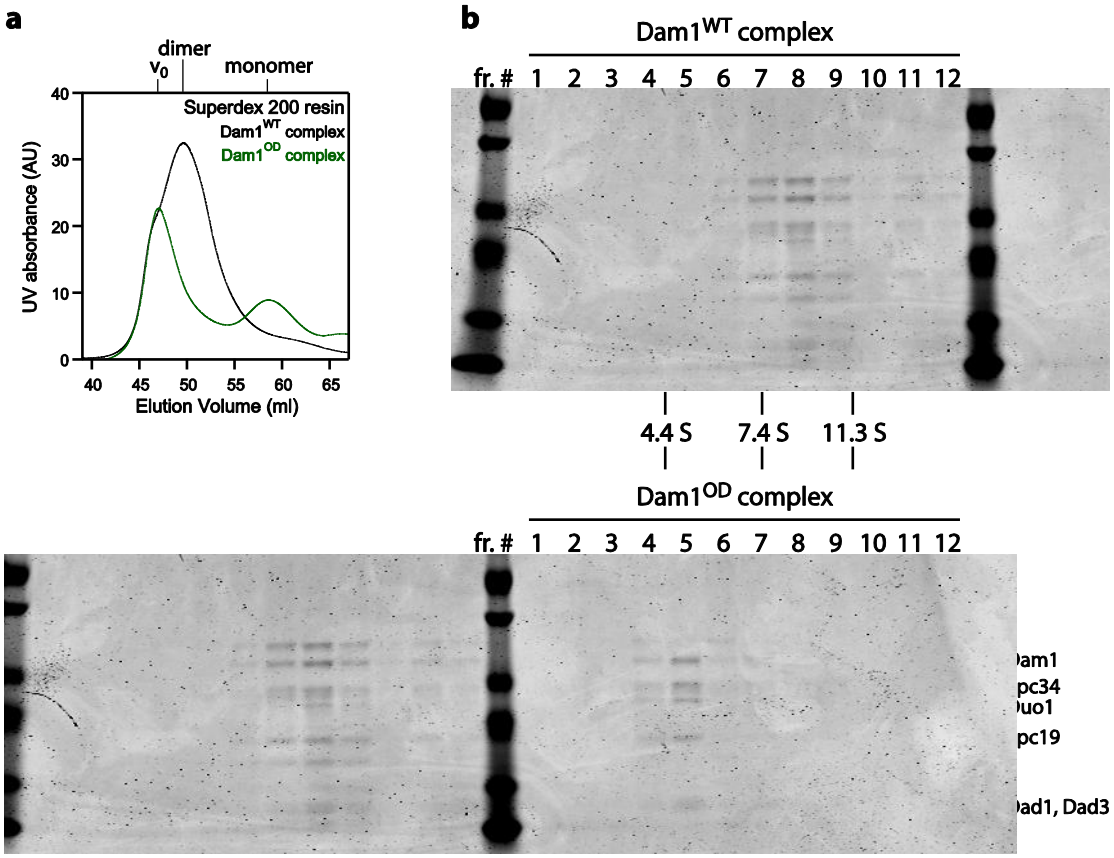

Supplementary Figure 3. The Dam1^{OD} complex does not dimerize in solution.
(a) Elution profiles from size-exclusion chromatography experiments performed on the wild-type (R_S 8.9 nm; WT, black trace) and oligomerization-deficient (R_S 7.3 nm; OD, green trace) Dam1 complexes. Stokes radii were determined using a standard curve generated from BSA, catalase, ferritin, thyroglobulin. (b) Coomassie-stained SDS-PAGE gels show velocity sedimentation analyses for Dam1^{WT} (9.1 S; upper gel) and Dam1^{OD} (4.9 S; lower gel) complexes. BSA, aldolase, and catalase were used as standards. Data from (a) and (b) were combined to estimate molecular weight[1]. In solution, the Dam1^{WT} complex is primarily dimeric (observed species is ~340 kDa; monomers are predicted to be ~200 kDa), while the Dam1^{OD} complex is monomeric (observed ~150 kDa; predicted ~140 kDa monomer).

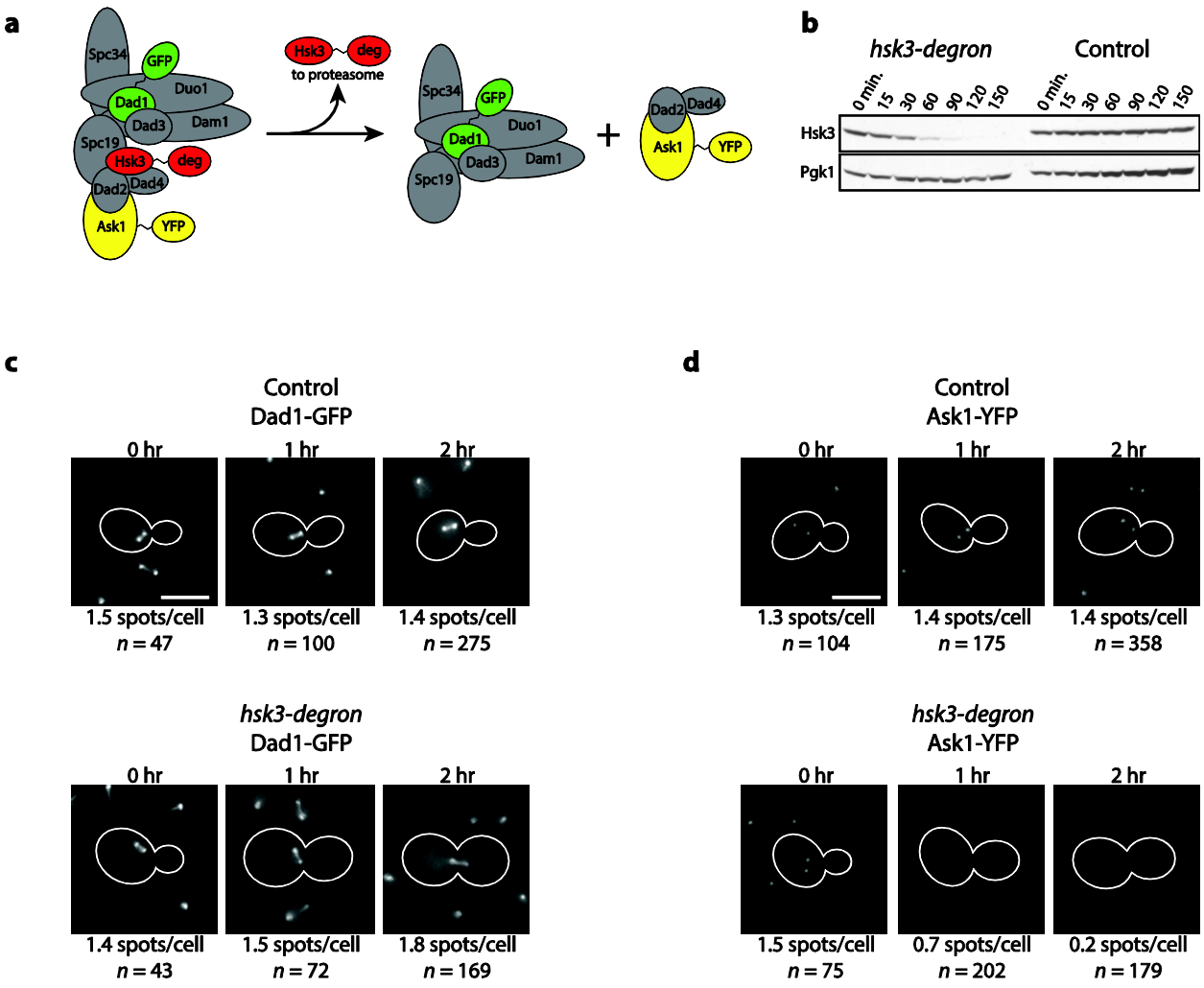

Supplementary Figure 4. An inducible Hsk3 degron system separates the microtubule-binding module of the Dam1 complex from the oligomerization module *in vivo*.
(a) Diagram of the Hsk3 degron system and the predicted separation of the two structural modules of the Dam1 complex *in vivo*. (b) Western blot shows the degradation kinetics of Hsk3 upon addition of auxin to asynchronously growing *hsk3-degron* and control cells; anti-V5 antibody was used to detect a V5 epitope in the degron tag. Pgk1 was used as a loading control. (c) Representative images of Dad1-GFP in mitotic control (top) and *hsk3-degron* (bottom) cells, in samples taken at the designated times following the addition of auxin to the growth medium. Below each image is the average number of detected spots per cell and the total number of cells observed. Images at 2 hours after addition of auxin are reproduced from Fig. 5a. Scale bar is 5 µm; image contrast was adjusted equally. (d) Analogous to (c), but shows representative images of Ask1-YFP in control and *hsk3-degron* cells.

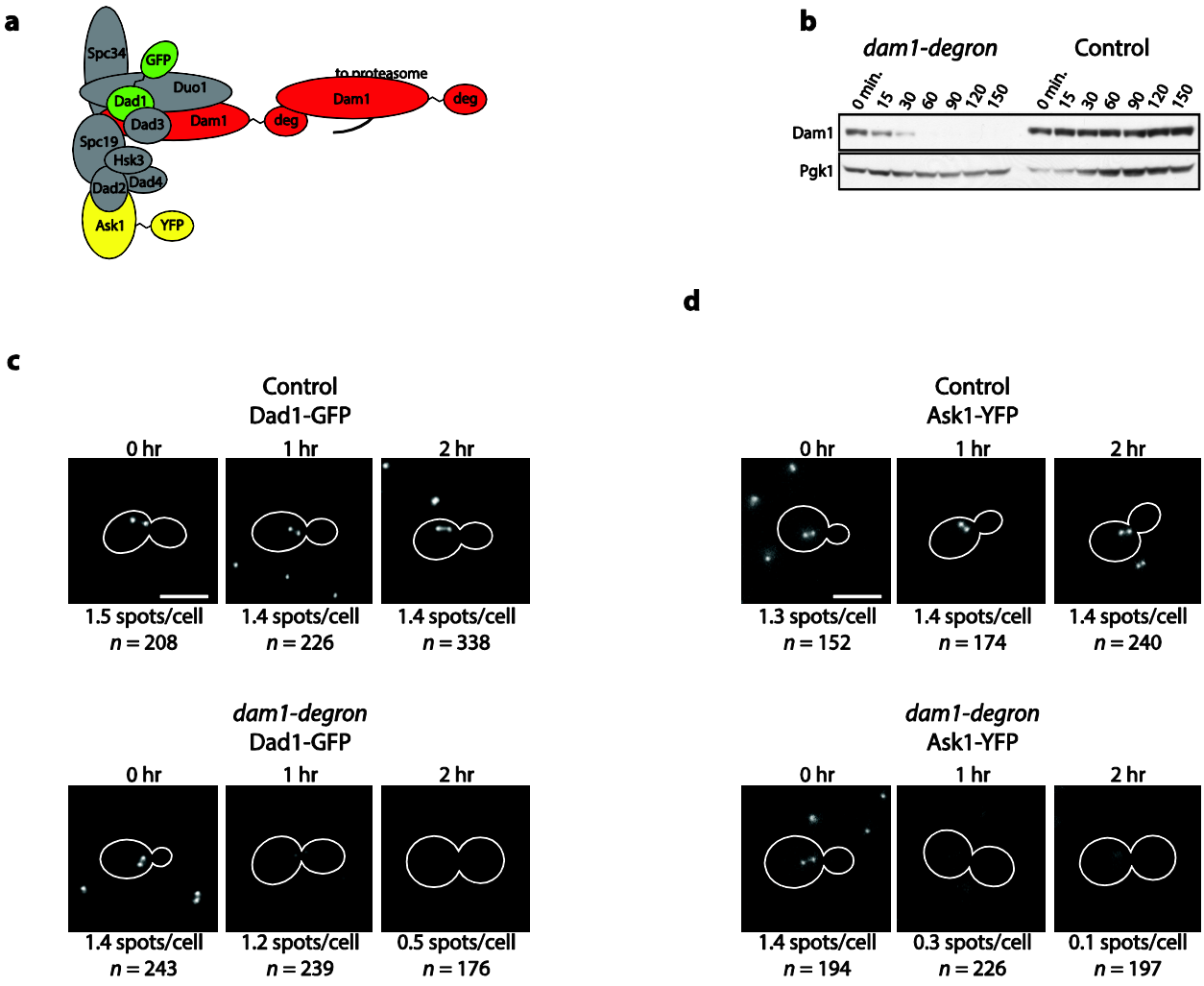

Supplementary Figure 5. Targeting the degron system to the Dam1 protein disrupts localization of both structural modules of the Dam1 complex.

Analogous to Figure S4. (a) Diagram of the Dam1 degron system. (b) Western blot shows degradation kinetics of Dam1 upon addition of auxin to asynchronously growing *dam1-degron* and control cells; anti-V5 antibody was used to detect a V5 epitope in the degron tag. Pgk1 was used as a loading control. Representative images and quantification of spots per cell for Dad1-GFP (c) and Ask1-YFP (d), as in Figure S4. Images of *dam1-degron* cells at 2 hours after addition of auxin are reproduced from Fig. 5a. Contrast was adjusted equally for comparison with images shown in Figure S4; scale bars are 5 µm.

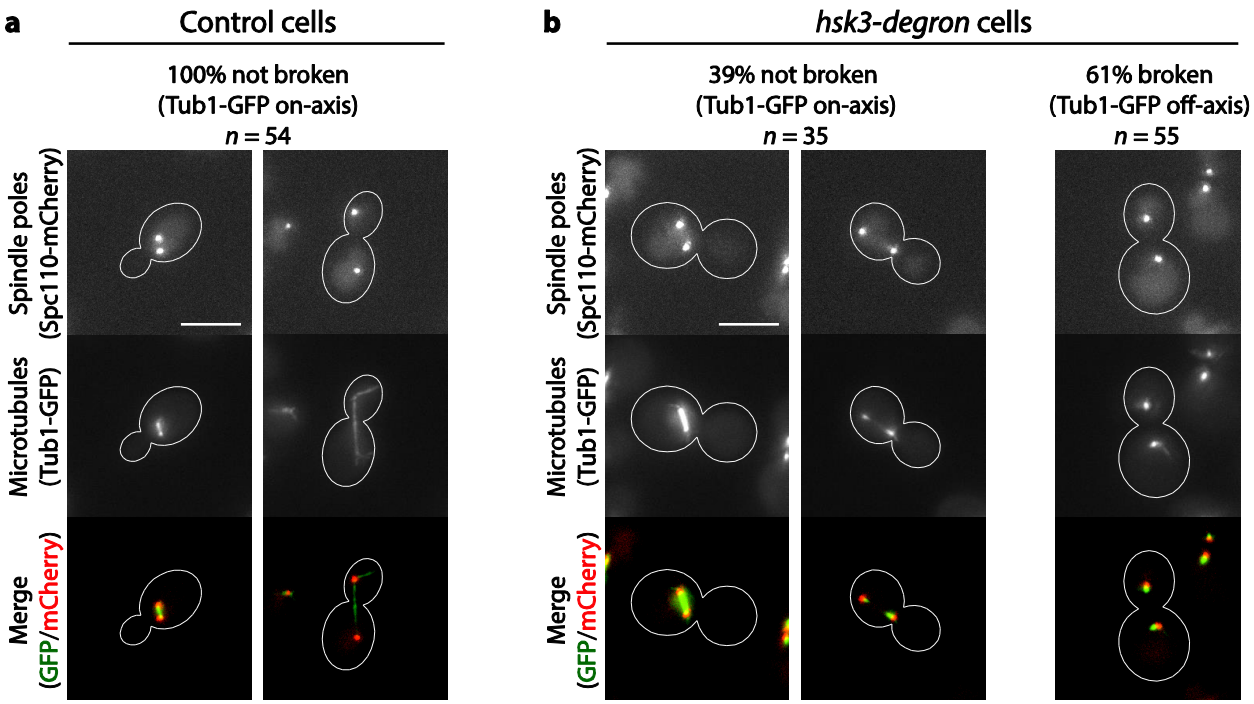

Supplementary Figure 6. Hsk3-depleted cells exhibit spindle morphology defects.
Spindle poles (Spc110-mCherry) and microtubules (Tub1-GFP) were imaged in asynchronously growing control cells (a) and *hsk3-degron* cells (b) after treatment with auxin for 2 hours. Spindle morphology was quantified by the spatial distribution of Tub1-GFP along the spindle axis. Spindles were considered broken if Tub1-GFP fluorescence was not oriented along the spindle axis. Image contrast was adjusted identically in (a) and (b); scale bars are 5 µm.

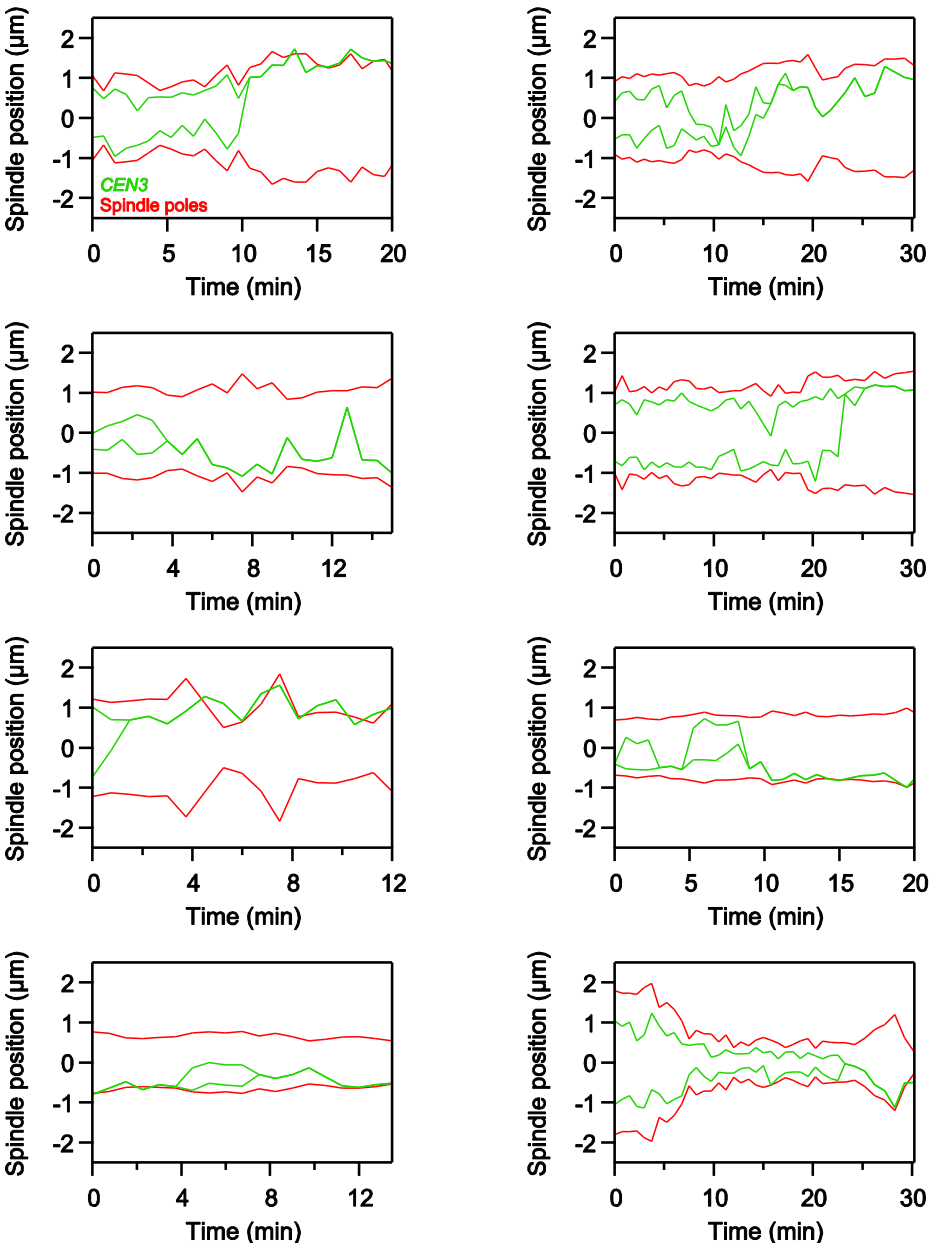

Supplementary Figure 7. Examples of kinetochore-microtubule attachment failure during *CEN3* biorientation in Hsk3-depleted cells.

Related to Figure 6c; additional traces of position versus time are shown for spindle poles (red) and *CEN3* spots (green).

Strain	Genotype	Figure
SBY3	*MAT***a** *ura3-1 leu2-3,112 his3-11 trp1-1 can1-100 ade2-1 bar1-1*	-
SBY12423	*MAT***a** *NUF2-GFP:HIS3MX6 SPC110-mCherry:hphMX HSK3-3V5-IAA7:KanMX ura3-1:OsTIR1-9myc:URA3 BAR1 ade3*Δ	Figure 6
SBY12425	*MAT***a** *NUF2-GFP:HIS3MX6 SPC110-mCherry:hphMX HSK3-3V5-IAA7:KanMX BAR1 ade3*Δ	Figure 6
SBY12501	*MAT***a** *pCUP1-GFP12-LacI2:HIS3 CEN3::33LacO:KanMX SPC110-mCherry:hphMX HSK3-3V5-IAA7:KanMX ura3-1:OsTIR1-9myc:URA3 bar1-1 ade3*Δ	Figure 7
SBY12503	*MAT***a** *pCUP1-GFP12-LacI12:HIS3 CEN3::33LacO:KanMX SPC110-mCherry:hphMX HSK3-3V5-IAA7:KanMX bar1-1 ade3*Δ	Figure 7
SBY12504	*MAT***a** *HSK3-3V5-IAA7:KanMX ura3-1:OsTIR1-9myc:URA3 ASK1-YFP:HIS3*	Figure 5a-b, S3
SBY12506	*MAT***a** *HSK3-3V5-IAA7:KanMX ASK1-YFP:HIS3*	Figure 5a-b, S3
SBY12662	*MAT***a** *HSK3-3V5-IAA7:KanMX ura3-1:OsTIR1-9myc:URA3 DAD1-GFP:KanMX6*	Figure 5a-b, S3
SBY12664	*MAT***a** *HSK3-3V5-IAA7:KanMX DAD1-GFP:KanMX6*	Figure 5a-b, S3
SBY12729	*MAT***a** *DAM1-3V5-IAA7:KanMX ura3-1:OsTIR1-9myc:URA3 ASK1-YFP:HIS3*	Figure 5c, S4
SBY12731	*MAT***a** *DAM1-3V5-IAA7:KanMX ASK1-YFP:HIS3*	Figure 5c, S4
SBY12733	*MAT***a** *DAM1-3V5-IAA7:KanMX ura3-1:OsTIR1-9myc:URA3 DAD1-GFP:KanMX6*	Figure 5c, S4
SBY12735	*MAT***a** *DAM1-3V5-IAA7:KanMX DAD1-GFP:KanMX6*	Figure 5c, S4
SBY12750	*MAT***a** *ura3-1::TUB1-GFP:URA3 SPC110-mCherry:hphMX HSK3-3V5-IAA7:KanMX his3-11:OsTIR1:HIS3*	Figure S5
SBY12751	*MAT***a** *ura3-1::TUB1-GFP:URA3 SPC110-mCherry:hphMX HSK3-3V5-IAA7:KanMX*	Figure S5

Supplementary Table 1. Genotypes of strains generated for use in this study.
All strains contain the markers of SBY3 unless otherwise noted.

Supplementary References

1. Siegel LM, Monty KJ. Determination of molecular weights and frictional ratios of proteins in impure systems by use of gel filtration and density gradient centrifugation. Application to crude preparations of sulfite and hydroxylamine reductases. *Biochim Biophys Acta* **112**, 346-362 (1966).